INTERNATIONAL JOURNAL OF RESEARCH IN COMPUTER APPLICATIONS AND ROBOTICS
ISSN 2320-7345

THREE-PHASE HYBRID TRANSFORMER WITH BUCK-BOOST MATRIX-REACTANCE CHOPPER

K.M.Ahamed Refai[1], G.Ananth Gifton[2], R.Sarathkumar Kithiyon[3], A.PremKumar[4], S.Immanuel Prabaharan[5]

[1, 2,3,4.] *Students ananthgifton1@gmail.com*
[5.] *Assistant Professor* imman.nce@gmail.com
Electronics and Communication Engineering Department, Chandy Engineering College, Tuticorin, Tamil Nadu, India

Abstract: - The parameters of electrical energy such as voltage amplitude are very important, particularly from the viewpoint of the final consumer and sensitive loads connected to the grid. The dynamic states in the power grid deep voltage sags and swells might cause faults and defects in sensitive loads. This paper deals with a three-phase hybrid transformer (HT) without dc energy storage to compensate voltage sags and swells and to protect sensitive loads against the rapid and extensive changes in supply voltage amplitude. The analyzed HT contains two main units: the first one is the conventional electromagnetic transformer, realizing an electromagnetic coupling, and the second one is the buck–boost matrix- reactance chopper, realizing an electrical coupling in the HT unit. In the presented solution, output voltage is transformed in two ways electromagnetically and electrically. This paper presents an operational description, the theoretical analysis, and the experimental test results from a 2-kVA laboratory model. On the basis of the authors' research, it can be stated that the HT makes it possible to compensate deep voltage sags (deeper than 50% of nominal source voltage) and over voltages (up to 140% of nominal source voltage) while maintaining good dynamic properties. The main advantages of the proposed solution, in comparison to other conventional solutions, are the ability to control the output voltage in the range of 0.66–3.5*US*, good dynamics (transient state during source voltage *uS* amplitude change is shorter than 10 ms), and galvanic separation between source and load (such as in the case of the conventional electromagnetic transformer).

Index Terms: - AC chopper, ac voltage stabilizer, ac–ac power conversion, power quality, voltage control.

I. INTRODUCTION

THE DYNAMIC states in a power grid, caused by faults, rapid load changes, switching effects, and atmospheric discharges, generate undesirable effects for the end user, such as voltage sags and interruptions [1]. In the case of sensitive loads, poor power quality causes failures or defects in devices as a result, large financial damages arise, particularly in automotive, pharmaceutical, and semiconductor industries [2]–[4]. Considering the above, there are various types of voltage sag/swell compensators that mitigate the unwanted effects on

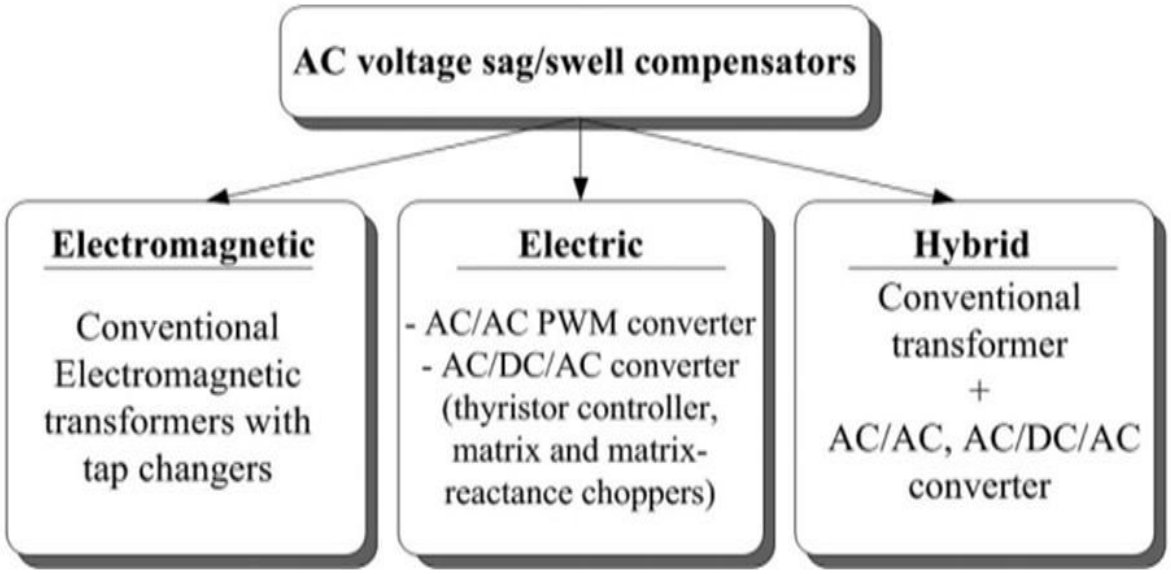

Figure. 1. Various types of ac voltage sag/swell compensators.

Supply [5]–[25] (see Fig. 1). The most popular group of voltage compensators are electromagnetic devices based on a conventional transformer (electromagnetic coupling) with a tap changer [8]. The ac voltage sag/swell compensators based on electromechanical or thyristor tap changer solutions have major defects, particularly poor dynamics, step changes, and a narrow
range of output voltage adjustment [26], [27]. Moreover, the tap changers are often working in no-load mode; thus, to get variable output voltage, it is necessary to disconnect the load. Additionally, stepwise changing cannot secure the precise regulation of output voltage at the required level (e.g., 230 or 115 V, depending on the power system). Because of the poor dynamics of ac voltage compensators with tap changers, a rapid response to voltage sags and swells is impossible. Another group of compensators is based on electric devices [6], [9]–[11] (with electrical coupling). These solutions guarantee good dynamic properties, but the major disadvantage is the lack of galvanic separation between supply source and load galvanic separation is a crucial issue in power system applications, particularly from the point of view of safety and matching of voltage level. The last group of ac voltage compensators for mitigating voltage amplitude fluctuations is based on hybrid solutions (with electromagnetic and electrical coupling), where a conventional electromagnetic transformer cooperates with a pulse width modulation (PWM) ac/ac converter [5], [12]–[24]. In these solutions, the electromagnetic coupling is realized by the transformer, and the electrical coupling is realized by the PWM ac/ac converter. In the literature, one can find many different solutions of hybrid compensators. The major disadvantage of a circuit described in [12] is the possibility to compensate only voltage sags (up to 50% of US). Another solution with similar properties to the above is described in [13]. The PWM ac/ac or ac/dc/ac converter cooperates with a transformer, but the circuit cannot compensate over voltages and does not guarantee galvanic separation between source and load. Galvanic separation between source and load is guaranteed in the circuits described in [14]; however, these solutions work with high frequency link and often need many bidirectional switches. Galvanic separation is guaranteed too in the case of the circuit described in [15]. However, the mechanical tap changer reduces the dynamic properties of this solution. An often encountered circuit for voltage sag/swell compensation, which belongs to the hybrid ac voltage compensator family, is the dynamic voltage restorer (DVR) [16]–[23]. One of its main advantages is the ability to compensate deep voltage sags (40% of source voltage sag) and over voltages (30% of source overvoltage) [19]–[23].

TABLE I
PROPERTIES OF VARIOUS TYPES OF AC VOLTAGE SAG/SWELL COMPENSATORS WITHOUT ENERGY STORAGE

	Electro-magnetic	Electric	Hybrid
Galvanic separation	YES	NO	YES/NO
efficiency η	> 97 %	> 90%	> 90%
Range of output voltage control (max.)	+/- 10 – 12 % U_S	0-100% U_S 0-350% U_S(MRC)	50-200% U_S
Voltage sag compensation	NO	YES (only MRC)	YES
Overvoltage compensation	NO	YES	YES
Output voltage change	steps	continuous	continuous
Dynamic	0,1 – 0,3 s / 10% U	< 20 ms / 10% U	< 20 ms / 10% U
kg / kVA (devices about. 100 kVA)	about 6 kg / kVA	about 0.1 kg / kVA	-

where: MRC – matrix-reactance chopper

A DVR equipped with dc energy storage also allows the compensation of interruptions [16]–[18]. The properties of various types of voltage sag/swell compensators, without energy storage, are presented in Table I [5]–[25], [28].The ac voltage compensators based on conventional electromagnetic transformers are characterized by a narrow range of change of output voltage and step regulation. The widest range of change of rms voltage transmittance, defined as

$$HU = \frac{UOUT}{UIN} \qquad (1)$$

is found on devices based on the matrix-reactance chopper (MRC) topology [6], [10], [28] (see Fig. 2), but these devices have no galvanic separation between source and load, which is crucial in power system applications. The group based on a hybrid solution (electromagnetic transformer and ac/ac converter) provides galvanic separation and a rather wide range of change of voltage transmittance ($0.5 \leq HU \leq 2$) (see Fig. 2).
To realize galvanic separation and compensation of deep voltage sags and over voltages, it is necessary to obtain a wider range of change of the voltage transmittance than what known hybrid solutions can provide (see Table I and Fig. 2).

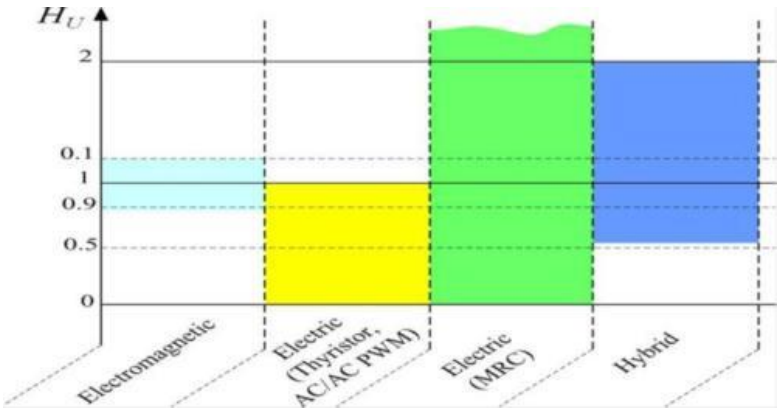

Figure. 2. Range of change of voltage transmittance

The analysis of power quality issues [29]–[31] shows that, in about 92% of all power system events, there are voltage sags with 40%–50% of the nominal value and with a duration from 2 to 30 periods. Only about 4% of sags occur with duration from 2 s to 10 min [29]–[31]. Taking into account the above and as an alternative to

known solutions, it is advisable to construct voltage compensators with galvanic separation between source and load and with a wide range of change of voltage transmittance.

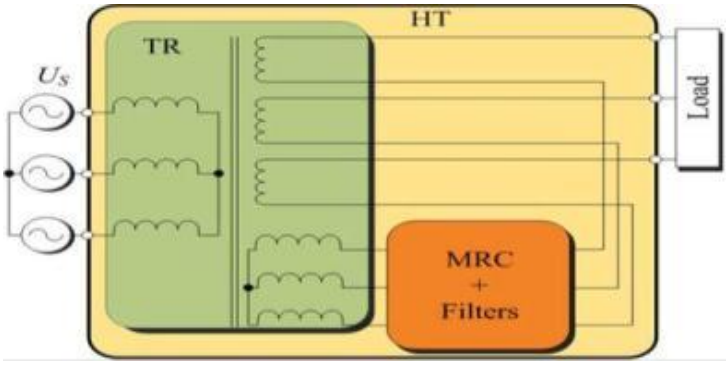

Figure. 3. Simplified scheme of three-phase HT.

To compensate the voltage sag deeper than 50% of *Us*, it is necessary to obtain a voltage transmittance of $H_U >$ 2.

This paper presents the steady- and transient-state properties of the three-phase voltage compensator. The arrangement consists of a transformer and buck boost MRC because of which this solution is called a hybrid transformer (HT) (see Fig. 3). A concept similar to the one presented in this paper is introduced in [5], where a single-phase transformer cooperates with a single-phase matrix ac chopper. The range of change of voltage transmittance obtained is 0.66 < *HU* < 2. This paper develops the concept presented in [5] by using a three-phase transformer and a different ac/ac converter topology a three phase buck–boost MRC instead of the ac/ac PWM matrix chopper with different properties. In this case the obtained range of change of the voltage transmittance is wider at 0.66 < *HU* < 3.5. Additionally, in comparison to [5], the authors have applied a different control circuit, based on the peak detection method [32]. This paper also extends the theoretical analysis (steady and dynamic states) presented in [5].

The described HT has a new topology (structure) and, in comparison to other hybrid devices, guarantees galvanic separation and the compensation of source voltage sags up to 28% of nominal voltage and over voltages up to 150% of nominal voltage. This range is much wider than in any known solution without energy storage [5]–[25], [28]. Taking into consideration the above, the described solution is an interesting alternative to conventional tap changer transformers and to other solutions without energy storage.

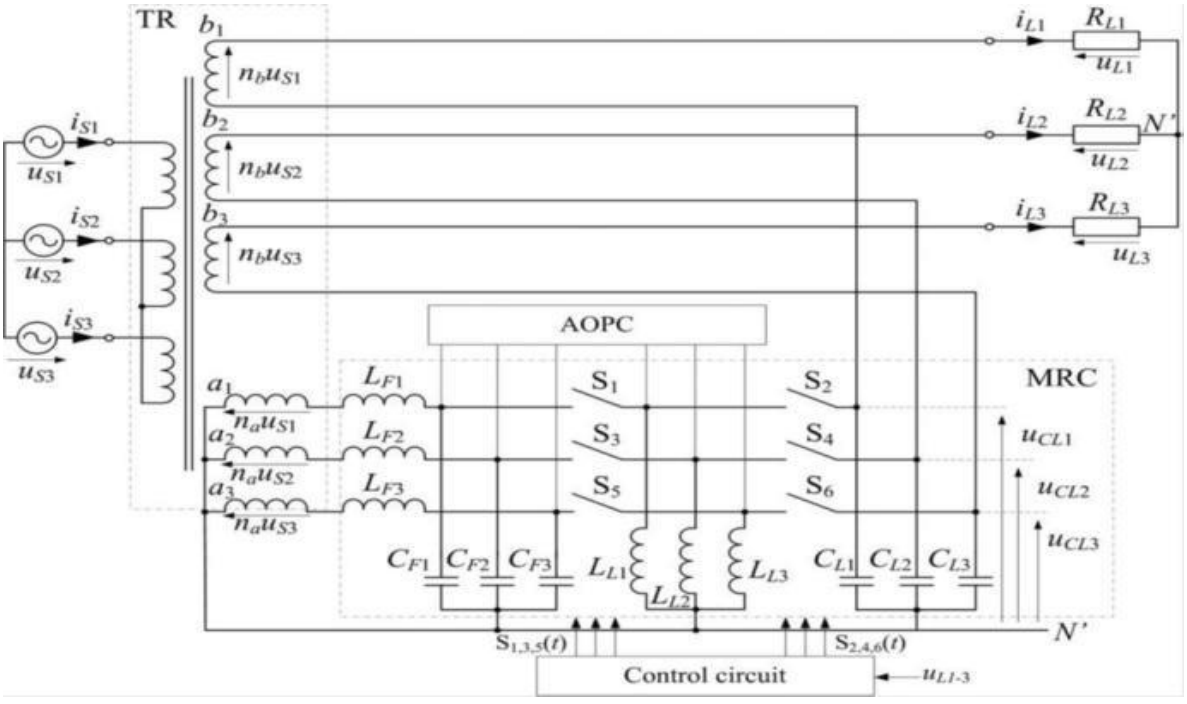

Figure. 4. Simplified schematic diagram of three-phase HT with ideal switches.

II. CIRCUIT AND OPERATION DESCRIPTION

A. Main Circuit

A schematic diagram of the considered three-phase HT with ideal switches (S1 - S6) and active overvoltage protection circuit (AOPC) [44] is shown in Fig. 4.

The described HT contains two main units: an electromagnetic transformer (TR) and a buck–boost MRC. As shown in Fig. 4, the primary windings are in Y-configuration. The main secondary windings (*a*1, *a*2, *a*3) of the TR also have a Y-configuration and, by input filter *LC*, are connected to a buck–boost MRC. The secondary phase windings (*b*1, *b*2, *b*3) are connected in series with the required phase output connectors of the MRC. The output rms voltages of the HT (*UL*1, *UL*2, *UL*3) are the sum of the rms secondary voltages (*nbUS*1, *nbUS*2, *nbUS*3) and the phase rms output voltages of the MRC (*UCL*1, *UCL*2, *UCL*3). The voltages for the first phase (*uS*1(*ωt*=0)) in the presented HT in complex form are given by

$$\underline{U}_{S1} = U_S \cdot e^{j0} \quad (2)$$

$$n_a\underline{U}_{S1} = -n_a U_S \cdot e^{j0} \quad (3)$$

$$n_b\underline{U}_{S1} = n_b U_S \cdot e^{j0} \quad (4)$$

$$\underline{U}_{CL1} = n_a U_S H_U^{b-b} \cdot e^{j0} \quad (5)$$

$$\underline{U}_{L1} = \underline{U}_{CL1} + n_b\underline{U}_{S1} \quad (6)$$

$$\left|\underline{H}_U^{b-b}\right| = \left|\frac{\underline{U}_{CL}}{n_a\underline{U}_s}\right| \approx \frac{D}{1-D} \quad (7)$$

where *na* and *nb* are the voltage ratios of windings *a*1,2,3 and *b*1,2,3, respectively, and are equal to *na*=4⁄3 and *nb*=2⁄3 [5], [33]–[40]; *Hb*−*b* is the voltage transmittance of buck–boost

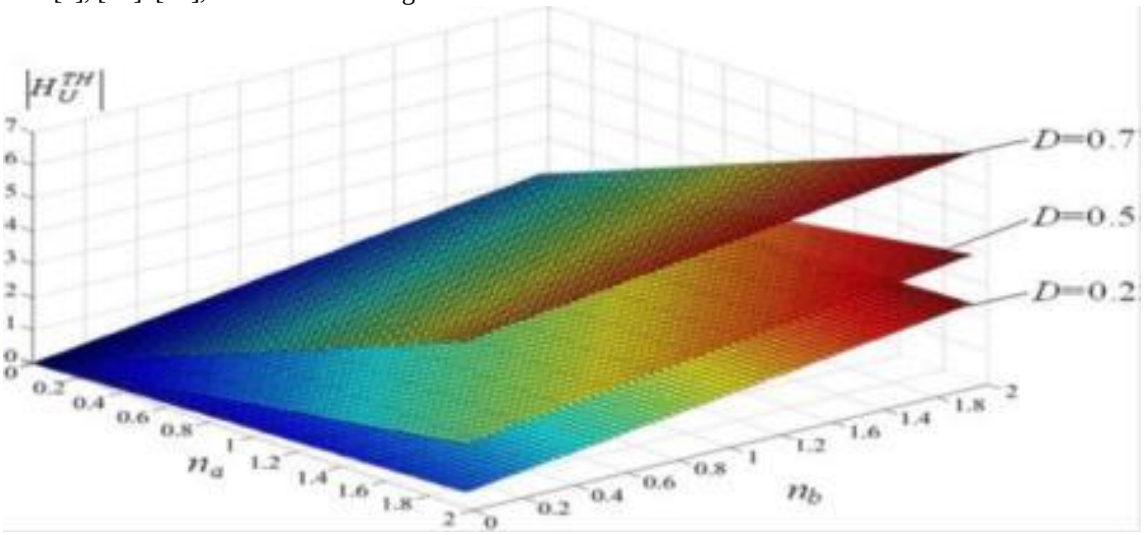

Figure. 5. Influence of change of TR voltage ratio *na* and *nb* on voltage transmittance of HT (*D* = 0.2, *D* = 0.5, and *D* = 0.7).

MRC. The output voltages of the MRC (*UCL*1, *UCL*2, *UCL*3) are dependent on the pulse duty factor *D* defined as follows:

D = *t*on/*TS* (*t*on is the time-on of switches S1, S3, and S5, and *TS* is the switching period). Taking into account (2)–(7), the voltage transmittance of the HT can be described as (8). For *D* = 0.7, the output voltage *UL* is approximately 3.5 times greater than the source voltage *US*. When the duty cycle is *D* < 0.2, then output voltage *UL* is less than source voltage *US*. In nominal operation conditions, the voltage transmittance of the HT is equal to 1, which means that the output voltage of the HT is *UL* = *US* and *D* = 0.2

$$\underline{H}^{TH} \quad \left|\underline{U}_L\right| \quad \left|\frac{\underline{U}_{CL} + n_b\underline{U}_S}{\underline{U}_S}\right| \approx \frac{n_a D}{-D} + n_b. \quad (8)$$

The voltage transmittance is dependent not only on the pulse duty factor *D* but also on the voltage ratios *na* and *nb* of TR (8). The influence of the change of the TR winding voltage ratio (*na*, *nb*) on the range of change of voltage transmittance is shown in Fig. 5.

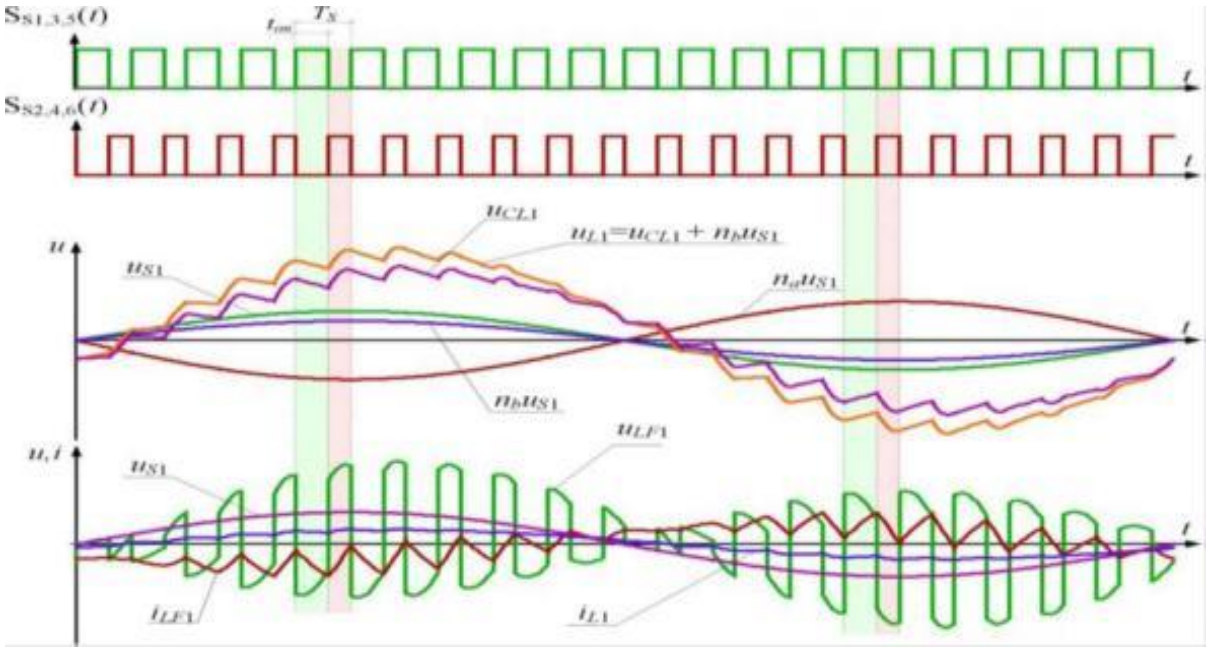

Figure. 6. Idealized voltage and current time waveforms in HT circuit for pulse duty factor D = 0.6 and switching frequency fs = 500 Hz.

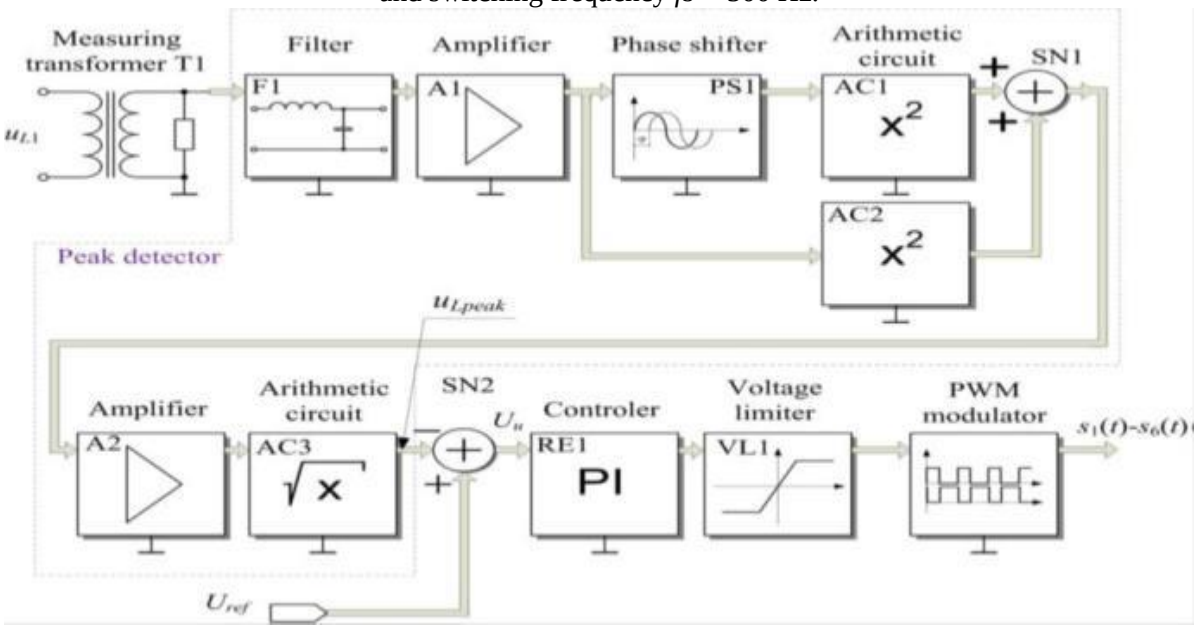

Figure. 7. Control circuit of HT.

As shown in Fig. 5, by using suitable voltage ratios, it is possible to obtain various ranges of change of voltage transmittances and, thus, various capabilities for the compensation of voltage sags and swells. Exemplary idealized voltage and current time waveforms illustrating the operation of the HT are shown in Fig. 6.

According to (6), the *UL* output voltage of the HT is the sum of the *UCL* output voltage of the MRC and the *nbUS* secondary voltage of the TR (see Fig. 6). The buck–boost MRC inverts the *UCL* phase output voltage of the MRC in relation to the *naUS* input voltage of the MRC. For this reason, to correctly sum the voltages (U_{CL} and n_bU_S), the n_aU_S voltage must be shifted by π in relation to the U_S source voltage.

B. Control Circuit

The buck–boost MRC in the considered HT is controlled by the PWM method. A schematic block diagram of the control circuit of the HT is shown in Fig. 7 [40].The control circuit contains three main units: the peak detector unit to detect voltage amplitude fluctuation, PI controller and PWM modulator. The function realized by the peak detector is described by [32]

$$u_{Lpeak} = \sqrt{(U_L \sin(\omega t))^2 + (U_L \cos(\omega t))^2} \quad (9)$$

where *uLpeak* is an output signal of the peak detector unit (see Fig. 7). The input signal of the peak detector—load voltage *uL* is distributed as two signals. One of them is shifted by $\pi/2$ according to (9). Both signals are then squared and summed. Finally, to obtain the output signal *uLpeak*, the square root of this sum is obtained [32].

III. THEORETICAL ANALYSIS

The static properties of the considered HT were analyzed on the basis of the averaged state-space method (10) [41], the space vector, and the d-q transformation methods (13) [42], [43]. A theoretical analysis of the dynamic properties was made on the basis of the small-signal model and Laplace transformation (24) [41]

$$\dot{\bar{X}} \cong A(D)\bar{x} + B(D)\mu s \quad (10)$$

A. Steady-State Analysis with Open Feedback Loop

According to (10), the averaged state-space equation of the analyzed HT (see Fig. 4) in matrix form can be described as (11), shown at the bottom of the page [40]. Taking into account (11), the averaged circuit model of the considered HT can be constructed as shown in Fig. 8 [40]. The analyzed circuit is assumed to be symmetric. Transformation into the D-Q coordinate system is realized in two steps. In the first one, three-phase voltages and currents are defined as space vectors (12), shown at the bottom of the page, and in the second step, space vectors are transferred into the D-Q coordinate system (13), shown at the bottom of the page [40]. The above variables are defined as follows:

$$\mathbf{x}_{ABC} = \begin{bmatrix} x_a \\ x_b \\ x_c \end{bmatrix} \quad (14)$$

$$\mathbf{x}_{SV} = \begin{bmatrix} x_0 \\ x_Z \\ x_P \end{bmatrix} \begin{matrix} \Leftarrow zero \\ \Leftarrow forward \\ \Leftarrow backward \end{matrix} \quad (15)$$

$$\mathbf{K} = \frac{2}{3}\begin{bmatrix} 1 & 1 & 1 \\ 1 & a^2 & a \\ 1 & a & a^2 \end{bmatrix} \quad (16)$$

$$a = e^{j\frac{2\pi}{3}} \quad (17)$$

$$\theta(t) = \pm \omega t + \theta_0. \quad (18)$$

A schematic diagram of the analyzed HT in the D-Q coordinate system is shown in Fig. 9.

$$\begin{bmatrix} \frac{di_{LF1}}{dt} \\ \frac{du_{CF1}}{dt} \\ \frac{di_{LL1}}{dt} \\ \frac{du_{CL1}}{dt} \\ \frac{di_{LF2}}{dt} \\ \frac{du_{CF2}}{dt} \\ \frac{di_{LL2}}{dt} \\ \frac{du_{CL2}}{dt} \\ \frac{di_{LF3}}{dt} \\ \frac{du_{CF3}}{dt} \\ \frac{di_{LL3}}{dt} \\ \frac{du_{CL3}}{dt} \end{bmatrix} \cong \underbrace{\begin{bmatrix} 0 & \frac{-1}{L_{F1}} & 0 & 0 & 0 & 0 & 0 & 0 & 0 & 0 & 0 & 0 \\ \frac{1}{C_{F1}} & 0 & \frac{-D}{C_{F1}} & 0 & 0 & 0 & 0 & 0 & 0 & 0 & 0 & 0 \\ 0 & \frac{D}{L_{L1}} & 0 & \frac{-(1-D)}{L_{L1}} & 0 & 0 & 0 & 0 & 0 & 0 & 0 & 0 \\ 0 & 0 & \frac{1-D}{C_{L1}} & \frac{-1}{R_{L1}C_{L1}} & 0 & 0 & 0 & 0 & 0 & 0 & 0 & 0 \\ 0 & 0 & 0 & 0 & 0 & \frac{-1}{L_{F2}} & 0 & 0 & 0 & 0 & 0 & 0 \\ 0 & 0 & 0 & 0 & \frac{1}{C_{F2}} & 0 & \frac{-D}{C_{F2}} & 0 & 0 & 0 & 0 & 0 \\ 0 & 0 & 0 & 0 & 0 & \frac{D}{L_{L2}} & 0 & \frac{-(1-D)}{L_{L2}} & 0 & 0 & 0 & 0 \\ 0 & 0 & 0 & 0 & 0 & 0 & \frac{1-D}{C_{L2}} & \frac{-1}{R_{L2}C_{L2}} & 0 & 0 & 0 & 0 \\ 0 & 0 & 0 & 0 & 0 & 0 & 0 & 0 & 0 & \frac{-1}{L_{F3}} & 0 & 0 \\ 0 & 0 & 0 & 0 & 0 & 0 & 0 & 0 & \frac{1}{C_{F3}} & 0 & \frac{-D}{C_{F3}} & 0 \\ 0 & 0 & 0 & 0 & 0 & 0 & 0 & 0 & 0 & \frac{D}{L_{L3}} & 0 & \frac{-(1-D)}{L_{L3}} \\ 0 & 0 & 0 & 0 & 0 & 0 & 0 & 0 & 0 & 0 & \frac{1-D}{C_{L3}} & \frac{-1}{R_{L3}C_{L3}} \end{bmatrix}}_{\mathbf{A}} \begin{bmatrix} i_{LF1} \\ u_{CF1} \\ i_{LL1} \\ u_{CL1} \\ i_{LF2} \\ u_{CF2} \\ i_{LL2} \\ u_{CL2} \\ i_{LF3} \\ u_{CF3} \\ i_{LL3} \\ u_{CL3} \end{bmatrix}$$

$$+ \underbrace{\begin{bmatrix} \frac{n_a}{L_{F1}} & 0 & 0 \\ 0 & 0 & 0 \\ 0 & 0 & 0 \\ \frac{-n_b}{R_{L1}C_{L1}} & 0 & 0 \\ 0 & \frac{n_a}{L_{F2}} & 0 \\ 0 & 0 & 0 \\ 0 & 0 & 0 \\ 0 & \frac{-n_b}{R_{L2}C_{L2}} & 0 \\ 0 & 0 & \frac{n_a}{L_{F3}} \\ 0 & 0 & 0 \\ 0 & 0 & 0 \\ 0 & 0 & \frac{-n_b}{R_{L3}C_{L3}} \end{bmatrix}}_{\mathbf{B}} \cdot \begin{bmatrix} u_{S1} \\ u_{S2} \\ u_{S3} \end{bmatrix}, \quad (11)$$

$$\mathbf{x}_{SV} = \mathbf{K}\mathbf{x}_{ABC}, \quad (12)$$

$$\mathbf{x}_{DQ} = \mathbf{x}_{SV} e^{j\theta(t)} \quad (13)$$

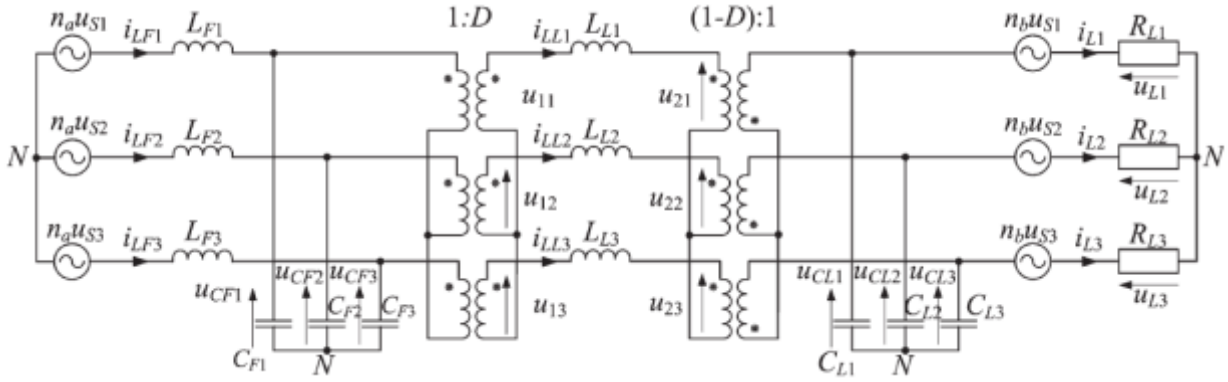

Figure. 8. Averaged circuit model of considered three-phase HT.

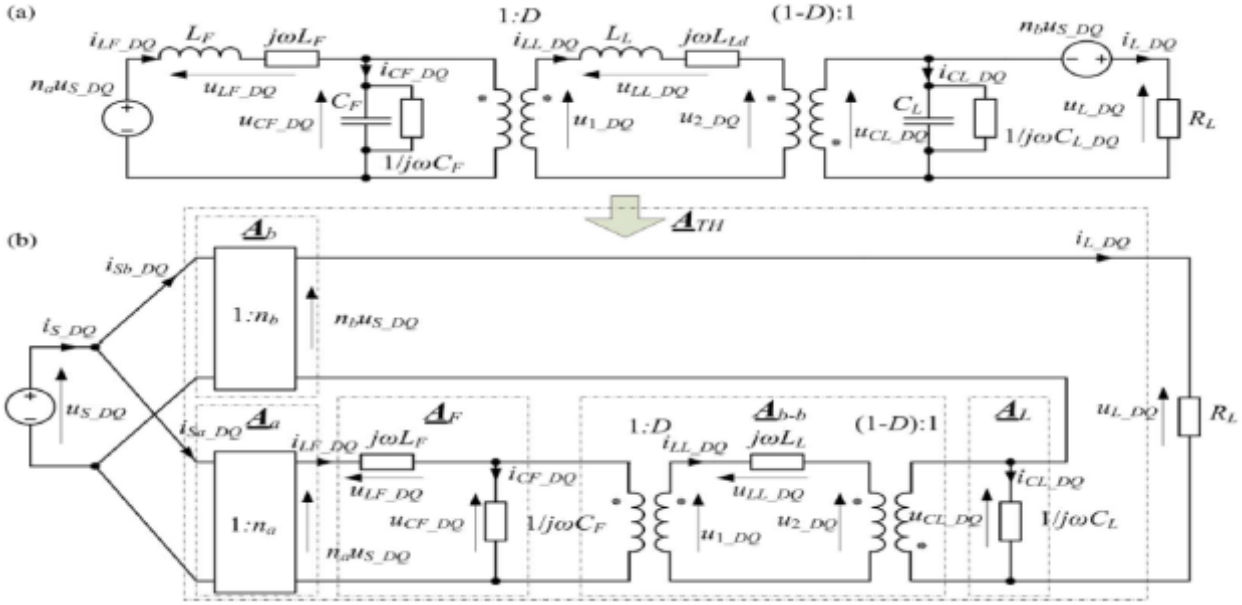

Figure. 9. Circuit model of considered HT in D-Q coordinate system. (a) General form. (b) In four-terminal description.

For steady-state analysis, a single-phase circuit model was divided into four-terminal networks [see Fig. 9(b)] [28], [33]– [37], [39], [40]. The four-terminal networks **A***a*, **A***F* , **A***b*−*b*, and **A***L* are connected in series and parallel–series with **A***b*. Taking into account the connections between four-terminal networks [see Fig. 9(b)], we can easily obtain the chain parameters of the considered HT

$$\begin{bmatrix} \underline{U}_{S\_DQ} \\ \underline{I}_{S\_DQ} \end{bmatrix} = \underline{\mathbf{A}}_{HT} \begin{bmatrix} \underline{U}_{L\_DQ} \\ \underline{I}_{L\_DQ} \end{bmatrix} = \begin{bmatrix} \underline{A}_{HT11} & \underline{A}_{HT12} \\ \underline{A}_{HT21} & \underline{A}_{HT22} \end{bmatrix} \begin{bmatrix} \underline{U}_{L\_DQ} \\ \underline{I}_{L\_DQ} \end{bmatrix} \quad (19)$$

$$\left|\underline{H}_U^{HT}\right| = \left|\frac{\underline{U}_L}{\underline{U}_S}\right| = \left|\frac{1}{\underline{A}_{HT11} + \underline{A}_{HT12}/R_L}\right| \quad (20)$$

$$\arg \underline{H}_U^{HT} = \arg\left(\frac{1}{\underline{A}_{HT11} + \underline{A}_{HT12}/R_L}\right) \quad (21)$$

$$\lambda_S = \frac{P_S}{S_S} = \cos\left[\arg\left(\frac{\underline{A}_{HT11}R_L + \underline{A}_{HT12}}{\underline{A}_{HT21}R_L + \underline{A}_{HT22}}\right)\right]. \quad (22)$$

The static characteristics as a function of the pulse duty factor *D* of the magnitude of the voltage transmittance (20), the phase of voltage transmittance (21), and the input power factor (22) are collected with simulation and experimental test results and shown in Section IV (see Fig. 17).

B. Dynamic State with Open Feedback Loop

The analyses of the dynamic properties of the open feedback loop circuit are based on the averaged state-space small signal model [40]. It is assumed that all variables have two components: a constant component (the

averaged value in the switching period *TS*), which is marked by an uppercase letter, and a perturbation component marked by a lowercase letter, straddled by the symbol "^"

$$i_{LF} = I_{LF} + \hat{}i_{LF},\ u_{CF} = U_{CF} + \hat{}u_{CF},\ i_{LL} = I_{LL} + \hat{}i_{LL},\ u_{CL} = U_{CL} + \hat{}u_{CL},\ d = D + \hat{}\,d. \quad (23)$$

On the basis of the averaged state-space method, the small signal state-space equations in the matrix form are expressed as

$$\frac{d}{dt}(\mathrm{X} + \hat{}\mathrm{x}) \approx \mathrm{A}\hat{}\mathrm{x} + \mathrm{B}\hat{}\mathrm{u} + [(\mathrm{A}_1 - \mathrm{A}_2)\mathrm{X} + (\mathrm{B}_1 - \mathrm{B}_2)\mathrm{U}]\hat{d} \quad (24)$$

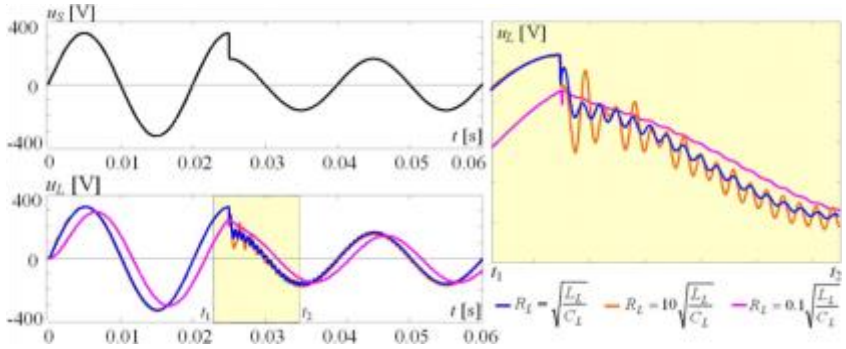

Figure. 10. Exemplary voltage time waveforms during µS supply voltage 50% step-down.

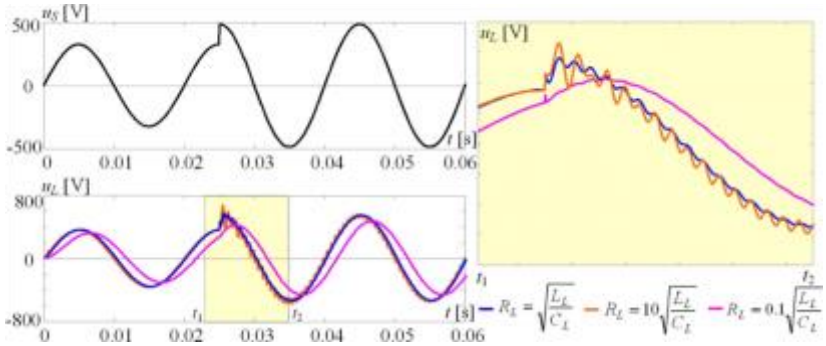

Figure. 11. Exemplary voltage time waveforms during µS supply voltage 50% step-up.

Where **A**1 and **A**2 are the circuit state matrices in the ON state (switches S1,3,5 are on, and switches S2,4,6 are off) and OFF state (switches S1,3,5 are off, and switches S2,4,6 are on), respectively, and **B**1 and **B**2 are the input matrices in the ON state and OFF state. According to (24), the Laplace transform of the small-signal state-space equation is expressed as

$$s\hat{\mathbf{x}}(s) = \mathbf{A}\hat{\mathbf{x}}(s) + \mathbf{B}\hat{\mathbf{u}}_S(s) + [(\mathbf{A}_1 - \mathbf{A}_2)\mathbf{X} + (\mathbf{B}_1 - \mathbf{B}_2)\mathbf{U}_S]\hat{d}(s) \quad (25)$$

$$u_L(s) = \mathbf{C}\hat{\mathbf{x}}(s) + \mathbf{D}\hat{\boldsymbol{u}}_S(s) \quad (26)$$

Solving (25) and (26), we obtain

$$\hat{X}(s) = (sI - A)^{-1} \times \{B\hat{u}_S(s) + [(A_1 - A_2)X + (B_1 - B_2)U_S]\hat{d}(s)\} = G_{\hat{X},\hat{u}_S}(s)u_s(s) + G_{\hat{X},\hat{d}}(s)\hat{d}(s) \quad (27)$$

$$\hat{u}_L(s) = [CG_{\hat{X},\hat{u}_S}(s) + D]\hat{u}_S(s) + [CG_{\hat{X},\hat{d}}(s)]\hat{d}(s) = G_{\hat{u}L,\hat{u}S}(s)\hat{u}_S(s) + G_{\hat{u}L,\hat{d}}(s)\hat{d}(s) \quad (28)$$

where **G**^**x**,^**u***S* is the state variable-supply voltage transmittance (29),**G**^**x**,^ *d* is the state variable-control signal transmittance (30), **G**^*uL*,^**u***S* is the load voltage-supply voltage transmittance (31), and **G**^*uL*, ^ *d* is the load voltage-control signal transmittance (32)

$$\mathbf{G}_{\hat{\mathbf{x}},\hat{\mathbf{u}}_S} = \frac{\hat{\mathbf{x}}(s)}{\hat{\mathbf{u}}_S(s)} \quad (29)$$

$$\mathbf{G}_{\hat{\mathbf{x}},\hat{d}} = \frac{\hat{\mathbf{x}}(s)}{\hat{d}(s)} \quad (30)$$

$$\mathbf{G}_{\hat{u}_L,\hat{\mathbf{u}}_S} = \frac{\hat{u}_L(s)}{\hat{\mathbf{u}}_S(s)} \quad (31)$$

$$\mathbf{G}_{\hat{u}_L,\hat{d}} = \frac{\hat{u}_L(s)}{\hat{d}(s)}. \quad (32)$$

The exemplary calculation of u_L load voltage time waveforms during a *us* supply voltage 50% step-down and a 50% step-up (31) and in an open feedback loop circuit is shown in Figs. 10 and 11, respectively. The transient time (see Figs. 10 and 11) is about 20 ms during the 50% step-up and step-down of supply voltage amplitude.

This provides good dynamic properties and a quick response of the considered HT to rapid changes of source voltage *us*.

C. Circuit with Closed Feedback Loop

Taking into account the model in Fig. 9 and control circuit in Fig. 7, we can obtain a substitute model of the considered HT with a closed-loop feedback (see Fig. 12). Based on the above and after linearization, a substitute scheme of the presented HT in s-domain (see Fig. 13) has been constructed. It is assumed that the Laplace transfer function of each block is described by

$$G_{PI}(s)| = \frac{\Delta D(s)}{\Delta U_u(s)} = K_P\left(1 + \frac{1}{T_I s}\right) \quad (33)$$

$$G_F(s) = \frac{1}{s^2 L_F C_F + s R_F C_F + 1} \quad (34)$$

$$G_{b-b}(s) = \frac{\Delta U_{CL}(s)}{\Delta U_{CF}(s)} \cong \frac{D}{1-D} \cong k_{b-b} \quad (35)$$

$$G_a(s) = \frac{n_a U_S(s)}{U_S(s)} = n_a \quad (36)$$

$$G_b(s) = \frac{n_b U_S(s)}{U_S(s)} = n_b \quad (37)$$

$$G_{peak\_det}(s) = \frac{U_L(s)}{U_{L\_peak}(s)} = 1. \quad (38)$$

Having regard to the connections between each block (see Fig. 13), we can easily obtain the block diagram (see Fig. 14) which is more convenient to analyze.

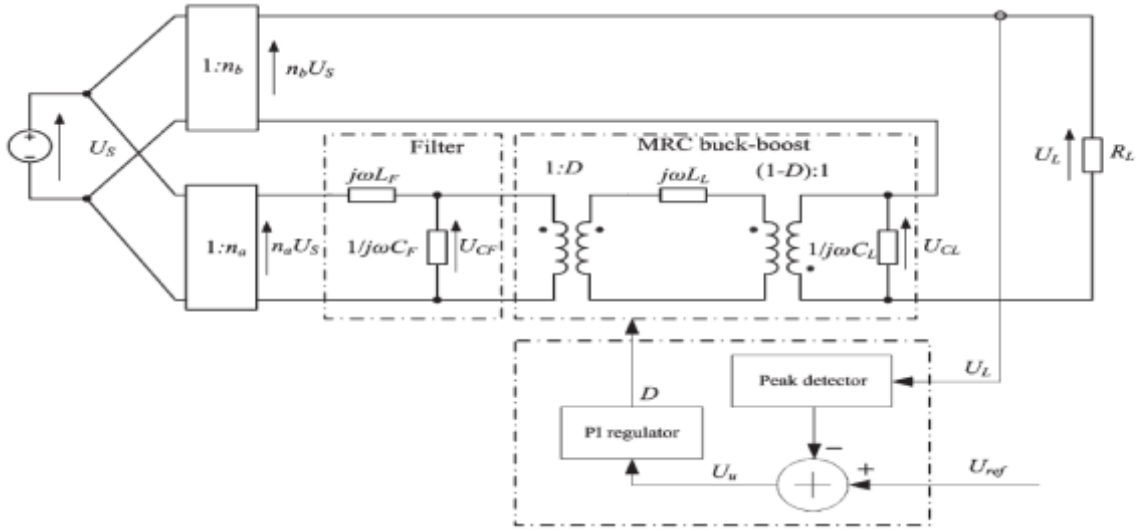

Figure. 12. Model of considered HT with control circuit.

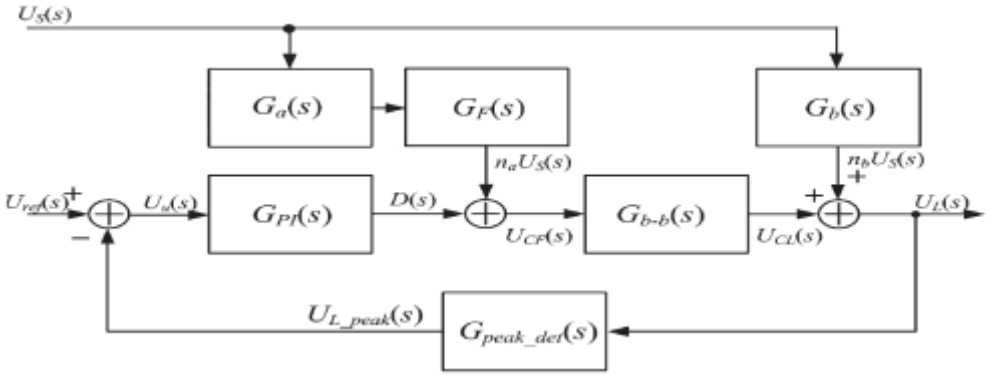

Figure. 13. Substitute block diagram of presented HT with control circuit,

Where *GPI*(*s*) is the transfer function of PI regulator, *Ga*(*s*) and *Gb*(*s*) are transfer functions of TR windings *a* and *b*, *GF* (*s*) is the transfer function of input filter, *Gb*−*b*(*s*) is the transfer function of buck–boostMRC, and *Gpeak_det*(*s*) is the transfer function of peak detector.

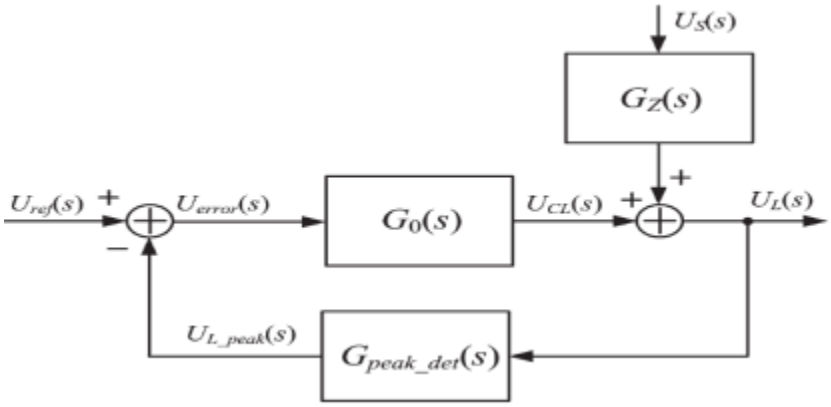

Figure. 14. Schematic diagram of analyzed HT in Laplace domain.

Each Laplace transfer function of the schematic from Fig. 14 is described by

$$GZ(s) = nb + \frac{nak_{b\_b}}{s2LFCF + sRFCF + 1} \tag{34}$$

$$G0(s) = \frac{\Delta U_{CL}(s)}{\Delta U_{error}(s)} GPI(s) \cdot G_{b-b}(s) \tag{35}$$

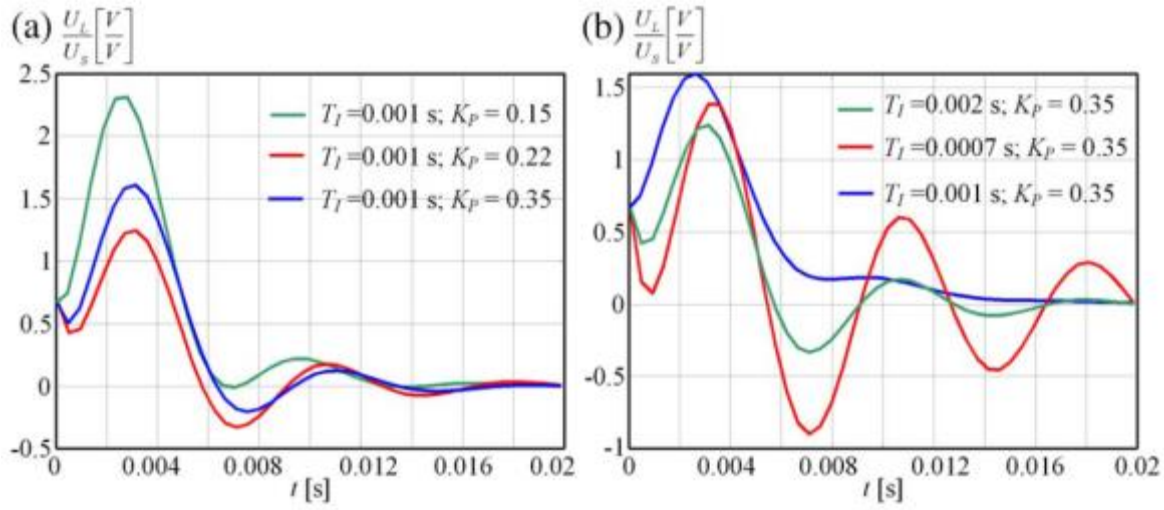

Figure. 15. Time waveforms of HT response to a step change disturbance for various settings of PI regulator, where Ti is the integration time and Kp is the gain factor.

Taking into account the above, the main Laplace transmittance of the HT, the control error transfer function, and the disturbance transfer function with closed feedback loop are defined by (41)–(43), respectively

$$G_{TH}(s) = \frac{\Delta U_L(s)}{\Delta U_{ref}(s)} = \frac{G_O(s)}{1 + G_O(s)} \tag{41}$$

$$G_{error}(s) = \frac{\Delta U_{error}(s)}{\Delta U_{ref}(s)} = \frac{1}{1 + G_O(s)} \tag{42}$$

$$G_{dist}(s) = \frac{\Delta U_L(s)}{\Delta U_S(s)} = \frac{G_Z(s)}{1 + G_O(s)} \tag{43}$$

where *GTH* is the main Laplace transmittance of the HT, *Gerror* is the control error transfer function, and *Gdist* is the disturbance transfer function. The response of the analyzed circuit (see Fig. 14) to a disturbance step change for various PI regulator parameter settings is shown in Fig. 15.

As is visible from Fig. 15, the control system used guarantees a rapid reaction, shorter than one source voltage period, to step changes of disturbances understood as voltage sag/swell. The best results are obtained for PI parameters: *Ti* = 0.002 s and *Kp* = 0.35. For this reason, these values are set as the parameters of the PI regulator in experimental analysis.

IV. SIMULATION AND EXPERIMENTAL TEST RESULTS

A three-phase 2-kVA prototype, intended to correct mains voltage variations in the range of +50/ - 72%, has been built and tested in a closed-loop control condition. The main specification and components used are shown in Table II.

TABLE II
CIRCUIT PARAMETERS

Parameter	name	value	unit
n_a	voltage ratio	4/3	-
n_b	voltage ratio	2/3	-
L_F / L_L	MRC inductance	1	mH
C_F / C_L	MRC capacitance	10	µF
R_L	Load resistance	10 *	Ω
f_s	switching frequency	6	kHz
U_S	supply voltage	3x400 *	V
IGBT	Transistors IRG4PHUD	I_C=24 V_{CES}=1200	A V
AOPC	DC voltage limit	90	V

* experiment - R_L=60 Ω, U_S = 50 V

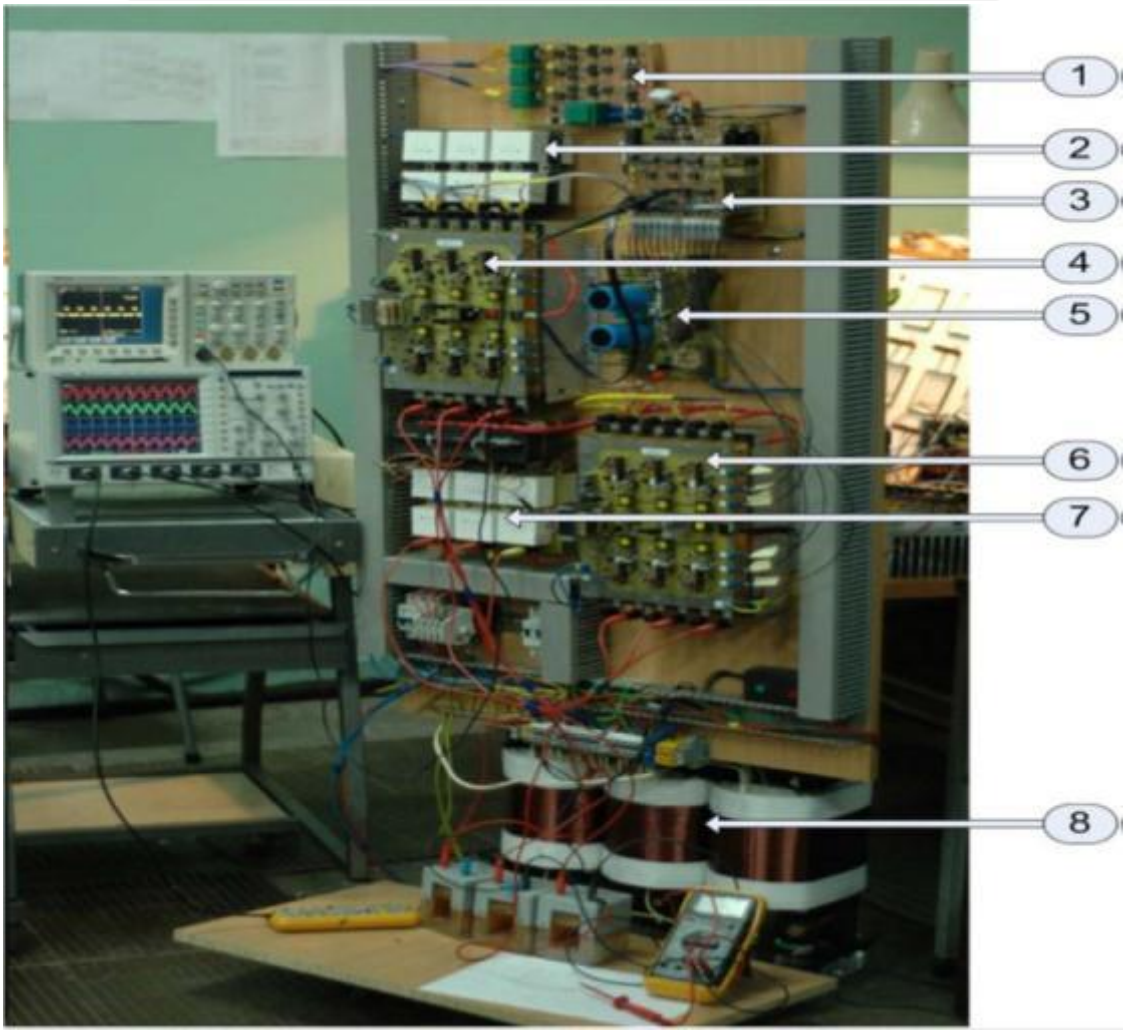

Figure. 16. Photograph of HT laboratory model. 1—Control unit (peak detector and PI regulators). 2—Input filter. 3—PWM unit. 4, 6—Power electronic switch modules (IGBT with drivers). 5—AOPC. 7—Output filter. 8—Threephase electromagnetic transformer TR.

The photograph of the experimental laboratory model of the described HT can be seen in Fig. 16. The buck–boost MRC is controlled via a PWM control strategy. The switching frequency is set to 6 kHz, and the "dead time" for commutation is set at 0.7 μs. The resonant frequency of filters is set to about 1/3 of the switching frequency (1/3 of *fs*). The capacitors used to build the laboratory model are ICEL metallized polypropylene film capacitors with capacitance 10 μF (4 × 2.5 μF/1200 V)—this value guarantees the good filtration of the input current higher harmonics. The bidirectional switches were implemented with two IRG4PHUD insulated gate bipolar transistors (IGBTs) (24 A/1200 V) connected in emitter-to-emitter configuration. Because the current of the MRC is higher during the compensation of voltage sag, the size of semiconductors was rated in relation to the maximum current during the compensation of source voltage sag. Additionally, the AOPC [44] was used to reduce the over voltages and current path of the inductor $LL1 - LL3$ currents at commutation ("dead time") states. Because of the phenomena of interaction between the main and control circuits, caused by the scattering of components in the mechanical construction of the experimental setup, a reduced supply voltage was used. The supply voltage range was set from 75 VRMS for swells and to 20 VRMS for sags. Experimentation is implemented using an analog and arithmetic integrated circuit for the proposed system. The same parameters were used as in the simulation and calculation.

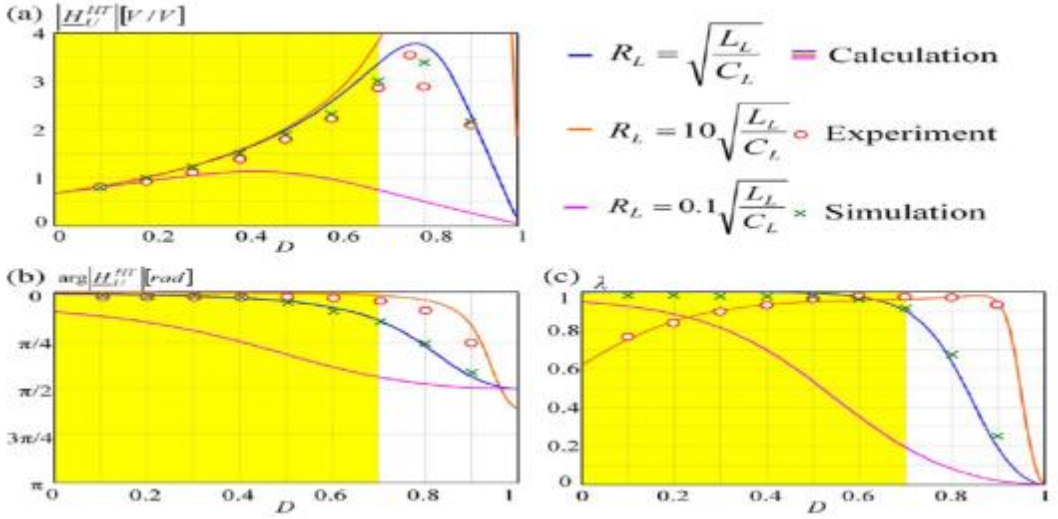

Figure. 17. Static characteristics of HT as a function of the pulse duty factor *D*. (a) Magnitude of voltage transmittance. (b) Phase of voltage transmittance. (c) Input power factor.

The presented results have been obtained for matching conditions described by

$$\sqrt{\frac{L_F}{C_F}} \approx \sqrt{\frac{L_L}{C_L}} \approx R_L \qquad (44)$$

The static characteristics of magnitude, phase of voltage transmittance, and input power factor as a function of pulse duty factor *D* are shown in Fig. 17(a)–(c), respectively. As one can see, the output voltage of the presented HT is smaller than the source voltage H <1 for D< 0.2 [see Fig. 18(a)]. In the case where the pulse duty factor D = 0.2, the output voltage of the HT is approximately equal to the source voltage (HU = 1).If D > 0.2, the output voltage is greater than the source voltage (HU > 1). The range of change of output voltage is from 0.66 *US* to about 3.5 *US*. Moreover, the best operating conditions are for conditions described by (44). Based on Fig. 17, we can define the useful working area. Because voltage transmittance and input power factor rapidly decrease for D>0.75 [see Fig. 17(a) and (c)], the useful working area should be from D = 0 to D = 0.75. This is also visible in the experimental voltage and current time waveforms for various values of duty pulse factor D (see Fig. 18). The range of change of output voltage is from 0.66 US [seeFig. 18(a)] to more than 3 US [see Fig. 18(c)]. For D > 0.75 [see Fig. 18(d)], output voltage UL is decreasing, and source current IS is much bigger than in the case when the pulse duty factor is less than 0.75, due to the resonance phenomena of MRC [28].

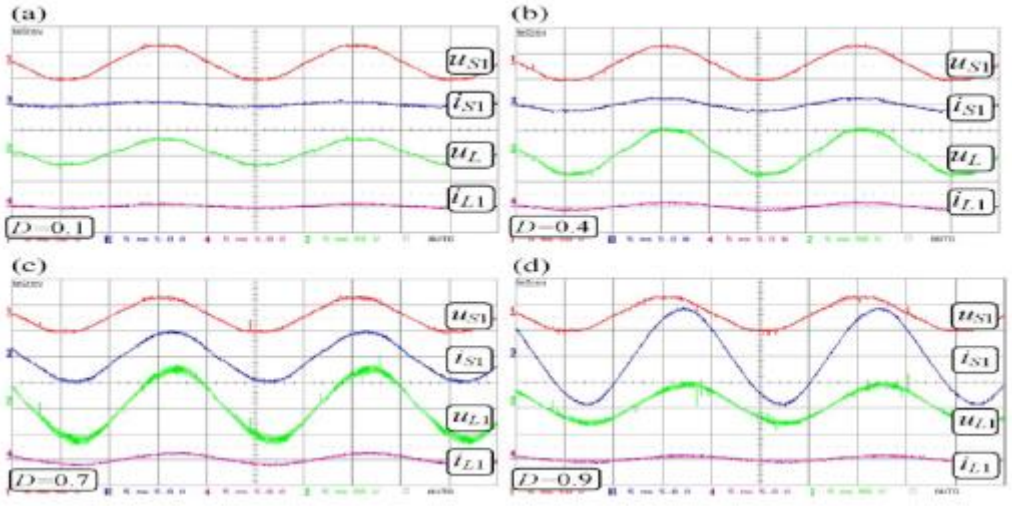

Figure. 18. Experimental source and load voltage and current time waveforms for (a) $D = 0.1$, (b) $D = 0.4$, (c) $D = 0.7$, and (d) $D = 0.9$.

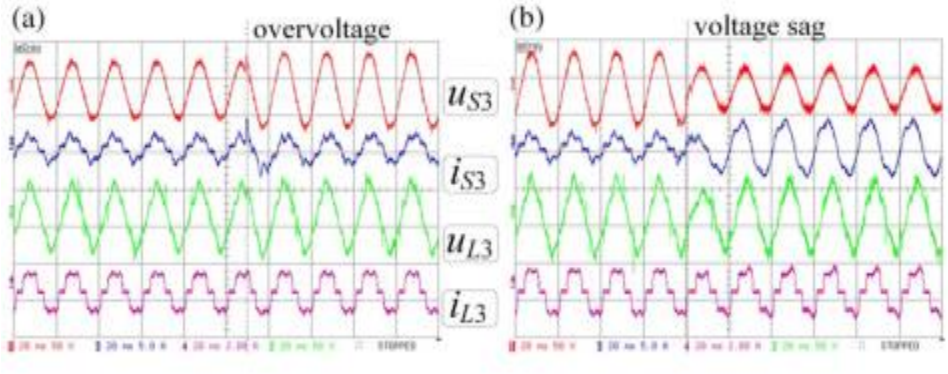

Figure. 19. Experimental voltage time waveforms for nonlinear load (three-phase rectifier) during (a) 140% *US* overvoltage and (b) 55% *US* voltage sag.

The load voltage UL is quasi-sinusoidal with the low component of the commutation (switching frequency fS = 6 kHz). Shown in Fig. 19 are the exemplary experimental time waveforms of source, load voltage, and current with nonlinear load (three-phase diode rectifier) during the overvoltage and voltage sag of the source voltage US in one of three phases of the HT. As can be seen, load voltage UL is kept at the nominal level, even with nonlinear load and during deep voltage sags and swells. The source current distortions for low values of pulse duty factor D are caused by the effect of the magnetizing current of the transformer.

V. CONCLUSION

In this paper, a three-phase HT for compensating deep voltage sag/swell has been presented. The operation and circuit have been described, and the main characteristics and time waveforms have been shown. The prototype was built for a rated power of 2 kVA. This prototype was operated using a control strategy based on the peak detection method and PWM modulation of the IGBTs. The acquired experimental results validate theoretical and simulation analysis. The proposed system is able to compensate voltage sags (up to 28%) and over voltages (up to 150%) of the source voltage US and keep the load voltage value (UL) at nominal level even with the rapid fluctuation of source voltage. The buck–boost MRC unit in the HT circuit is working even in nominal source voltage conditions. The proposed HT is an interesting alternative to other voltage compensators without energy storage, but only in the case of a circuit where the compensation of source voltage interrupts is not necessary. The next phase of the research will focus on building a more compact construction of the HT laboratory set with greater power (50 kVA) and with bidirectional IGBT's modules with better parameters. This will allow operation with a nominal voltage of (3 × 400 V), a 10-kHz switching frequency, and an estimated efficiency coefficient of about 90%.

APPENDIX

The chain parameters of the presented HT are shown at the bottom of the page.

$$A_{TH11} = \frac{1}{p_b + \frac{(-1+D)Dp_a}{-(-1+D)^2+\omega^2 M1}}$$

$$A_{TH12} = -\frac{i\omega(-D^2L_F + (-1+\omega^2 C_F L_F)L_L}{M2}$$

$$A_{TH21} = \frac{i\omega p_a^2(-D^2C_L + C_F\left((-1+D)^2 - \omega^2 C_L L_L\right))}{M2}$$

$$A_{TH22} = p_b + p_a\left(\frac{(-1+D)D(1+L1)}{M1} + \frac{D\left(D(p_a-p_b)+p_b\right) - p_a\omega^2 C_F L_L}{M2}\right)$$

$$M1 = -(-1+D)^2 + \omega^2\left((C_L(D^2L_F + L_L) + C_F L_F\left((-1+D)^2 - \omega^2 C_L L_L\right)\right)$$

$$M2 = (-1+D)(Dp_a - p_b) + p_b\omega^2(C_L(D^2L_F + L_L) + C_L L_L\left((-1+D)^2 - \omega^2 C_L L_L\right))$$

$$L1 = \frac{p_a^2\omega^2\left(-D^2L_F + (-1+\omega^2 C_F L_F)L_L\right)\left(-D^2C_L + C_F\left((-1+D)^2 - \omega^2 C_L L_L\right)\right)}{M1^2} - \left(p_b + \frac{(-1+D)Dp_a}{M1}\right)^2$$

REFERENCES

[1] J. Milanowi´c and I. Hiskansen, "Effect of load dynamics on power system damping," *IEEE Trans. Power Syst.*, vol. 10, no. 2, pp. 1022– 1028, May 1995.

[2] Z. Djokic, J. Desment, G. Vanalme, J. Milanovic, and K. Stockman, "Sensitivity of personal computer to voltage sags and short interruptions," *IEEE Trans. Power Del.*, vol. 20, no. 1, pp. 375–383, Jan. 2005.

[3] A. Falce, G. Matas, and Y. Da Silva, "Voltage sag analysis and solution for an industrial plant with embedded induction motors," in *Conf. Rec. IEEE IAS Annu. Meeting*, 2004, vol. 4, pp. 2573–2578.

[4] J. Duran-Gomez, P. Prased, N. Enjeti, and B. Woo B, "Effect of voltage sags on adjustable-speed drives: A critical evaluation on an approach to improve performance," *IEEE Trans. Ind. Appl.*, vol. 35, no. 6, pp. 1440– 1449, Nov./Dec. 1999.

[5] E. C. Aeloiza, P. N. Enjeti, L. A. Moran, and I. Pitel, "Next generation distribution transformer: To address power quality for critical load," in *Proc. IEEE PESC*, Jun. 2003, vol. 3, pp. 1266–2171.

[6] O. C. Montero-Hernandez and P. N. Enjeti, "Application of a boost acac converter to compensate for voltage sags in electric power distribution systems," in *Proc. IEEE PESC*, 2000, vol. 1, pp. 470–475.

A Brief Author Biography

G.Ananth Gifton[2] - He was born on 05 Sep 96 at Tuticorin. His father K.Ganasan, Mechanic in Port Trust. His mother G.Kasthuri, self-employee. He has completed hid school education at St.Lasalle Higher Sec. School. He is doing B.E in the Electronics and Communication field. His areas of interest are Electrical Instruments, VLSI, Embedded, multimedia, etc. He is having innovative mind. He is interested in writing software codes and doing many research works. On this occasion, I could like to submit my heartful thanks to our honourable Principle Dr.K.Sivakami Sundari, Our Head of the Department Mr.Prabaharan and our all department staffs for motivating me to publish this work.

R.Sarathkumar Kithiyon[3] - He was born on 06 jun 96 at Tuticorin. His father V.Raia,former . His mother R.Kanagavalli, self-employee. He has completed hid school education at Cladwell Higher Sec. School. He is doing B.E in the Electronics and Communication field. His areas of interest are VLSI, Electrical Instruments, Embedded, multimedia, etc,,. He is having innovative mind. He is interested in writing software codes and doing many research works. On this occasion, I could like to submit my heartful thanks to our honourable Principle Dr.K.Sivakami Sundari, Our Head of the Department Mr.Prabaharan and our all department staffs for motivating me to publish this work.